5658 *Inorg. Chem.* **2010**, *49*, 5658–5668
DOI: 10.1021/ic1005665

Inorganic Chemistry
Article

The Possible Role of 94−125 Peptide Fragment of Histone H2B in Nickel-Induced Carcinogenesis

Ana Mónica Nunes,[†] Kimon Zavitsanos,[†] Rebecca Del Conte,[‡] Gerasimos Malandrinos,*[,†] and Nick Hadjiliadis*[,†]

[†]*Department of Chemistry, University of Ioannina, 45110 Ioannina, Greece, and* [‡]*Magnetic Resonance Center, University of Florence, Via L. Sacconi 6, 0019, Sesto Fiorentino, Italy*

Received March 25, 2010

The molecular mechanism by which nickel carcinogenicity is exerted is not fully understood. However, it is believed to involve DNA damage and epigenetic effects in chromatin, resulting from metal binding to the cell nucleus. Histone nuclear proteins are the major candidates for metal binding not only due to their abundance but also due to the presence of strong binding sites within their sequence. In order to investigate the binding capacity of histone H2B toward Ni^{2+} ions, we synthesized the peptide Ac-IQTAVRLLLPGELAKHAVSEGTKAVTKYTSSK-Am ($H2B_{94-125}$) as a model of the C-terminal tail. Complexation of $H2B_{94-125}$ with Ni^{2+} starts at pH around 5 with the formation of a distorted octahedral complex. Over pH 8, this species shifts to a square-planar geometry, with the complete consumption of free Ni^{2+} ions at pH 10. The formation of the diamagnetic square-planar complex was further studied by means of NMR spectroscopy. On the basis of the NOE connectivities we determined a well-resolved solution structure for the binding site of the $H2B_{94-125}-Ni^{2+}$ complex, including residues $E_{12}LAKHAVS_{19}$. Interestingly, nickel binding strongly affects the C-terminal of the peptide, forcing it to approach the coordination plane. If such a structural alteration is able to occur under physiological conditions, it is highly possible that it interferes with the histone's physiological role and particularly with the ubiquitination process, taking place at Lys_{120}. We believe that these findings will assist in a better understanding of the role of histone H2B in the mechanisms of metal-induced toxicity and carcinogenesis.

Introduction

Histones are the nuclear proteins serving in DNA packaging within chromatin. The basic structural unit of chromatin is the nucleosome, which is formed by 146 DNA base pairs, wrapped around a protein octamer, consisting of heterodimeric pairs of four different nuclear histone proteins (H3, H4, H2A, and H2B).[1,2] Numerous studies have shown that the basic procedures of translation, transcription, and DNA repair are being controlled through post-translational modifications occurring in specific histone residues. There are at least eight types of known modifications, including acetylation, methylation, phosphorylation, ubiquitination, etc.[3] It is noteworthy that many of them act in a cooperative way, thus giving birth to the concept of the histone code.[1,3]

Several epidemiological studies have established nickel as a carcinogen for both humans and animals.[4] The proposed mechanisms of nickel-induced carcinogenesis involve reactive oxygen species (ROS) production, adjacent to DNA bases, due to formation of redox-active Ni^{2+}−histone complexes,[5] epigenetic effects that occur via malfunction of the histone code,[6] inhibition of DNA hypermethylation,[7] or interference with the calcium homeostasis processes.[8]

*To whom correspondence should be addressed. Fax: +302651008786. Tel: +302651008420. E-mail: nhadjis@uoi.gr (N.H.). Fax: +302651008786. Tel: +302651008407. E-mail: gmalandr@uoi.gr (G.M.).

(1) Elgin, S. C. R.; Workman, J. L. *Chromatin Structure and Gene Expression*, 2nd ed.; Oxford University Press: New York, 2000.
(2) Johns, E. W. *Biochem. J.* **1967**, *104*, (1), 78−82. Shaw, B. R.; Herman, T. M.; Kovacic, R. T.; Beaudreau, G. S.; Van Holde, K. E. *Proc. Natl. Acad. Sci. U. S. A.* **1976**, *73*, (2), 505−509. Noll, M.; Kornberg, R. D. *J. Mol. Biol.* **1977**, *109*, (3), 393−404. Finch, J. T.; Lutter, L. C.; Rhodes, D.; Brown, R. S.; Rushton, B.; Levitt, M.; Klug, A. *Nature* **1977**, *269*, (5623), 29−36. Luger, K.; Mader, A. W.; Richmond, R. K.; Sargent, D. F.; Richmond, T. J. *Nature* **1997**, *389*, (6648), 251−260.
(3) Kouzarides, T. *Cell* **2007**, *128*, (4), 693−705.
(4) IARC. *Monographs on the Evaluation and Carcinogenic Risks to Humans. Chromium, Nickel and Welding*; Lyon, 1990; Vol. *49*, p 677. Denkhaus, E.; Salnikow, K. *Crit. Rev. Oncol. Hematol.* **2002**, *42*, (1), 35−56. Sunderman, F. W.; Coulston, J. F., Eichhorn, G. L.; Fellows, J. A.; Mastromatteo, E.; Reno, H. T.; Samitz, M. H.; Curtis, B. A.; Vallee, B. L.; West, P. W.; McEwan, J. C.; Shibko, S. I.; , Boaz, T. D., Jr. In *Nickel*; National Academy of Sciences: Washington DC, 1975; p 277. Grimsrud, T. K.; Berge Steinar, R.; Martinsen, J. I.; Andersen, A. *J. Environ. Monit.* **2003**, *5*, (2), 190−197.
(5) *Nickel and Its Surprising Impact in Nature*; Sigel, A., Sigel, H., Sigel, R. K. O., Eds.; Wiley: Chichester, 2007; Vol. *2*.
(6) Broday, L.; Peng, W.; Kuo, M. H.; Salnikow, K.; Zoroddu, M.; Costa, M. *Cancer Res.* **2000**, *60*, (2), 238−241. Golebiowski, F.; Kasprzak, K. S. *Mol. Cell. Biochem.* **2005**, *279*, (1−2), 133−139.
(7) Lee, Y. W.; Klein, C. B.; Kargacin, B.; Salnikow, K.; Kitahara, J.; Dowjat, K.; Zhitkovich, A.; Christie, N. T.; Costa, M. *Mol. Cell. Biol.* **1995**, *15*, (5), 2547−2557. Govindarajan, B.; Klafter, R.; Miller Mark, S.; Mansur, C.; Mizesko, M.; Bai, X.; LaMontagne, K., Jr.; Arbiser Jack, L. *Mol. Med.* **2002**, *8*, (1), 1−8.
(8) Funakoshi, T.; Kuromatsu, K.; Kojima, S. *Res. Commun. Mol. Pathol. Pharmacol.* **1996**, *92*, (2), 245−252. Zamponi, G. W.; Bourinet, E.; Snutch, T. P. *J. Membr. Biol.* **1996**, *151*, (1), 77−90.; Salnikow, K.; Kluz, T.; Costa, M. *Toxicol. Appl. Pharmacol.* **1999**, *160*, (2), 127−132. Swierenga, S. H. H.; Whitfield, J. F.; Gillan, D. J. *J. Natl. Cancer Inst.* **1976**, *57*, (1), 125−129.

Published on Web 05/13/2010

In the last years, the interaction of histone peptide models comprising possible binding sites for the metal with Ni^{2+} ions has been extensively studied.[9−16] Our initial research concerned the interaction of Ni^{2+} ions with minimal peptide models of histone H2B, such as ELAKHA[17] and LAHYNK.[18] In order to obtain more realistic models and with the aim to study structural alterations induced by metal binding, we expanded our studies by dividing the whole H2B histone molecule in four peptide fragments ($H2B_{1-31}$, $H2B_{32-62}$, $H2B_{63-93}$, $H2B_{94-125}$).[19,20] In this paper we report our results concerning the $H2B_{94-125}$ peptide, Ac-IQTAVRLLLPGELAKH$_{16}$AVSEGTKAVTK$_{27}$YTSSK-Am, which is a model of the C-terminal tail of histone H2B. This peptide incorporates a part of the α3 helix of the histone fold domain and the C-terminus, which in the crystal structure of the nucleosome defines the outer limit of the core particle.[21] The latter suggests that this part of histone H2B is accessible to nickel ions and ranks it among the most likely binding sites within the protein.

Karaczyn et al.[22] have reported that in rat and human cells, Ni^{2+} induces truncation of histone H2B at two specific sites, thus forming H2B, which lacks Lys_{120}. The latter is a residue where a highly important post-translational modification takes place, i.e., ubiquitination.[23] This modification, which is a necessary first step for the methylation of Lys_4 of histone H3, has been shown to activate DNA transcription.[24] On the basis of their results,[22] they proposed a mechanistic pathway where Ni^{2+} is able to activate specific nuclear proteolytic enzymes, belonging to the calpain family, causing elimination of the modification site. However, in their later results they found a mechanistic independence between truncation and decrease of H2B ubiquitination.[25] This indicates that ubiquitination is being affected either through a mechanism involving the activation of other types of enzymes by Ni^{2+} or through the direct attack of the metal to the −ELAKHA− sequence of histone H2B, which was found earlier to have some binding capacity for it.[17]

Indeed, histone proteins are the most likely ligands for nickel ions inside the cell nucleus, not only due to the presence of strong binding sites within their sequence but also due to their abundance.[26] Likewise, it has been shown that metal binding to peptides and proteins may induce structural alterations, even in parts of the molecule that are distant from the binding site.[12,20,27] Therefore, it is possible that the nickel binding to His_{109} of histone H2B accounts for a conformational change in the fragment containing the modification site, hence disrupting the identification process by the appropriate enzyme.

In order to examine the above assumptions, we synthesized the peptide $H2B_{94-125}$, which comprises His_{16} as a possible binding site and Lys_{27}, where the ubiquitination occurs, and studied its interaction with Ni^{2+} ions by means of potentiometric titrations and spectroscopic techniques. Study of structural alterations upon nickel binding was attempted by NMR spectroscopy and only for the 4N $\{N_{Im}, 3N^{-}\}$ complex. The reason for that is that the available data in the literature suggest that the 4N complexes of nickel with peptides may be redox-active and induce ROS formation.[5] Besides that, Karaczyn et al.[22] had observed oxidative damage in the H2B molecule upon its treatment with nickel, consisting of oxidation of Met_{59} and Met_{62} to sulfoxides. In most coordination studies of peptides with nickel ions, the 4N complexes are being formed at alkaline pH.[15,17,19,20,28] However, it is possible that the environment in the whole protein enhances Ni^{2+} binding and assists in the 4N complex formation, even at physiological conditions, either due to multiple nonbonding interactions available there or due to a higher specificity of Ni^{2+} in producing a certain conformation.[29]

Experimental Section

Peptide Synthesis. The terminally blocked $H2B_{94-125}$ peptide Ac-IQTAVRLLLPGELAKHAVSEGTKAVTKYTSSK-Am was synthesized as described elsewhere.[19] The crude peptide was purified by gel filtration chromatography on Sephadex G-25 and HPLC, achieving a purity of over 98%. The peptide's identity was confirmed by means of an ESI-MS Sec (Micromass-Platform LC instrument).

Potentiometry. The potentiometric titrations were performed on a total volume of 3 mL samples at a ligand concentration of 5.0×10^{-4} M with a metal-to-ligand molar ratio of 1:1.1, using $NiCl_2$ as a source of Ni^{2+} ions. The excess of ligand was used in order to increase the reaction rate of nickel ions with $H2B_{94-125}$ in order to help the establishment of the final equilibrium to take place faster and increase the reliability of the measurements. The metal ion stock solutions were prepared from analytical grade reagents of $NiCl_2$, and their concentration was checked gravimetrically via the precipitation of oxinates. The titrations were

(9) Bal, W.; Lukszo, J.; Jezowska-Bojczuk, M.; Kasprzak, K. S. *Chem. Res. Toxicol.* **1995**, *8*, (5), 683−692.
(10) Zoroddu, M. A.; Schinocca, L.; Kowalik-Jankowska, T.; Kozlowski, H.; Salnikow, K.; Costa, M. *Environ. Health Perspect.* **2002**, *110*, 719−723.
(11) Bal, W.; Lukszo, J.; Bialkowski, K.; Kasprzak, K. S. *Chem. Res. Toxicol.* **1998**, *11*, (9), 1014−1023.
(12) Zoroddu, M. A.; Peana, M.; Medici, S. *Dalton Trans.* **2007**, (*3*), 379−384.
(13) Zoroddu, M. A.; Kowalik-Jankowska, T.; Kozlowski, H.; Molinari, H.; Salnikow, K.; Broday, L.; Costa, M. *Biochim. Biophys. Acta* **2000**, *1475*, (2), 163−168.
(14) Zoroddu, M. A.; Peana, M.; Kowalik-Jankowska, T.; Kozlowski, H.; Costa, M. *J. Chem. Soc., Dalton Trans.* **2002**, (*3*), 458−465.
(15) Mylonas, M.; Krezel, A.; Plakatouras, J. C.; Hadjiliadis, N.; Bal, W. *J. Chem. Soc., Dalton Trans.* **2002**, (*22*), 4296−4306.
(16) Karavelas, T.; Malandrinos, G.; Hadjiliadis, N.; Mlynarz, P.; Kozlowski, H.; Barsam, M.; Butler, I. *Dalton Trans.* **2008**, (*9*), 1215−1223.
(17) Karavelas, T.; Mylonas, M.; Malandrinos, G.; Plakatouras, J. C.; Hadjiliadis, N.; Mlynarz, P.; Kozlowski, H. *J. Inorg. Biochem.* **2005**, *99*, (2), 606−615.
(18) Panagiotou, K.; Panagopoulou, M.; Karavelas, T.; Dokorou, V.; Hagarman, A.; Soffer, J.; Schweitzer-Stenner, R.; Malandrinos, G.; Hadjiliadis, N. *Bioinorg. Chem. Appl.* **2008**, 257038.
(19) Zavitsanos, K.; Nunes, A. M.; Malandrinos, G.; Kallay, C.; Sovago, I.; Magafa, V.; Cordopatis, P.; Hadjiliadis, N. *Dalton Trans.* **2008**, (*44*), 6179−6187.
(20) Nunes, A. M. P. C.; Zavitsanos, K.; Del Conte, R.; Malandrinos, G.; Hadjiliadis, N. *Dalton Trans.* **2009**, (*11*), 1904−1913.
(21) Luger, K.; Mader, A. W.; Richmond, R. K.; Sargent, D. F.; Richmond, T. J. *Nature* **1997**, *389*, (6648), 251−260.
(22) Karaczyn, A. A.; Golebiowski, F.; Kasprzak, K. S. *Chem. Res. Toxicol.* **2005**, *18*, (12), 1934−1942.
(23) Zhu, B.; Zheng, Y.; Pham, A.-D.; Mandal, S. S.; Erdjument-Bromage, H.; Tempst, P.; Reinberg, D. *Mol. Cell* **2005**, *20*, (4), 601−611.
(24) Sun, Z.-W.; Allis, C. D. *Nature* **2002**, *418*, (6893), 104−108.
(25) Karaczyn, A. A.; Golebiowski, F.; Kasprzak, K. S. *Exp. Cell Res.* **2006**, *312*, (17), 3252−3259.
(26) Alberts, D.; Bray, D.; Lewis, J.; Raff, M.; Roberts, K.; Watson, J. D. *Molecular Biology of the Cell*, 3rd ed.; Garland: New York, 1994; p 335.
(27) Bal, W.; Wojcik, J.; Maciejczyk, M.; Grochowski, P.; Kasprzak, K. S. *Chem. Res. Toxicol.* **2000**, *13*, (9), 823−830.
(28) Mylonas, M.; Plakatouras, J. C.; Hadjiliadis, N. *Dalton Trans.* **2004**, (*24*), 4152−4160.
(29) Bal, W.; Chmurny, G. N.; Hilton, B. D.; Sadler, P. J.; Tucker, A. *J. Am. Chem. Soc.* **1996**, *118*, (19), 4727−4728. Yamashita, M. M.; Wesson, L.; Eisenman, G.; Eisenberg, D. *Proc. Natl. Acad. Sci. U. S. A.* **1990**, *87*, (15), 5648−5652. Regan, L. *Annu. Rev. Biophys. Biomol. Struct.* **1993**, *22*, 257−287.

Table 1. Acquisition Parameters of 2D and 3D NMR Experiments Performed with $H2B_{94-125}$ at 298 K

	acquired data points (nucleus)			spectral width (ppm)		
experiment	t_3	t_2	t_1	F_3	F_2	F_1
[^{1}H−^{1}H]-TOCSY[a]		2048 (^{1}H)	512 (^{1}H)		10 (^{1}H)	10 (^{1}H)
[^{1}H−^{1}H]-NOESY[a]		2048 (^{1}H)	576 (^{1}H)		10 (^{1}H)	10 (^{1}H)
[^{1}H−^{1}H]-NOESY[a]		2048 (^{1}H)	576 (^{1}H)		10 (^{1}H)	10 (^{1}H)
[^{1}H]−^{13}C-HSQC[a]		2048 (^{1}H)	384 (^{1}H)		10 (^{1}H)	80 (^{1}H)
[^{1}H]−^{15}N-HSQC[b]		1024 (^{1}H)	512 (^{15}N)		12 (^{1}H)	40 (^{15}N)
[^{1}H−^{1}H−^{15}N]-NHHa[b]	1024 (^{1}H)	128 (^{1}H)	16 (^{15}N)	13(^{1}H)	13 (^{1}H)	37 (^{15}N)

[a] Data acquired with a 600 or 700 MHz spectrometer. [b] Data acquired with a 700 MHz spectrometer.

performed at 298 K and at a constant ionic strength of 0.20 M KCl. All measurements were made with a MOLSPIN pH meter system, equipped with a 6.0234.100 combined electrode and a MOL-ACS microburet controlled by a computer. The pH readings were converted to hydrogen ion concentration as described elsewhere,[30] and a pK_w value of 13.76 was used for the ionization of water.

The evaluation of the measurements and calculations of the stability (log β_{fjk} for $M_fH_jL_k$) and protonation constants were performed using the general computer program HYPERQUAD.[31] Standard deviations (values) quoted were computed by HYPERQUAD and refer to random errors only. However, they are a good indication of the importance of the particular species in the equilibrium.

UV−Vis and CD Spectroscopy. Absorption and CD spectroscopy were conducted, at 298 K, using samples in the same concentration range as used for pH potentiometry. Any changes in the pH were monitored by a combined glass−silver chloride electrode over the range of 4 to 11.5. The solutions were manually titrated with small portions of either 0.2 M KOH or 0.2 M HCl solutions. The absorption spectra were recorded on a Perkin-Elmer Lambda 25 double-beam spectrophotometer, in the spectral range 250−800 nm. CD spectra are reported as the difference in molar absorptivities ($\Delta\varepsilon = \varepsilon_l - \varepsilon_\rho$) and were recorded on a JASCO J-810 spectopolarimeter in the 200−800 nm range.

NMR Spectroscopy. Sample Preparation. NMR samples were prepared at a concentration of 1−2 mM $H2B_{94-125}$ in 99.9% D_2O at pH 10.3 in the absence and presence of Ni^{2+} ions. Moreover, a series of 2D and 3D spectra were recorded at pH 2.5 for a 10 mM sample of $H2B_{94-125}$ in 10% D_2O and 90% H_2O. D_2O was purchased from Aldrich. The titration experiments of Ni^{2+} ions were made with aliquots of 0.1 M $NiCl_2$ in D_2O stock solution, reaching a peptide to Ni^{2+} ion molar ratio of 1:1. The pH was adjusted with small amounts of concentrated KOH and HCl deuterated solutions.

NMR Measurements. The NMR spectra were recorded on Bruker Avance spectrometers at 700 and 600 MHz, at 298 K. Water suppression was achieved with the use of presaturation or gradient pulse. A combination of total correlation spectroscopy (TOCSY), nuclear Overhauser enhancement spectroscopy (NOESY), rotating frame enhancement spectroscopy (ROESY), and ^{1}H−^{13}C-heteronuclear single quantum correlation (^{13}C-HSQC) at natural abundance was used to assign the resonances of both free and nickel-bound $H2B_{94-125}$, at pH 10.3. At this pH, the exchange rate of labile amide protons with bulk water is high and causes loss of their resonance signals. In order to facilitate the assignment procedure, a series of 2D and 3D spectra, including ^{1}H−^{15}N-HSQC and ^{1}H−^{1}H-^{15}N-NHHa for the free peptide, were recorded at pH 2.5, where the exchange rate is low and the amide proton signals are detectable. TOCSY experiments were acquired with a total spin-locking of 60 and 100 ms, using MLEV-17 mixing sequence, and NOESY was performed with 100 and 500 ms mixing times. For the ROESY spectra the respective time was 110 ms. All NMR data were processed using TOPSPIN Bruker software and analyzed using the CARA program.[32] All performed experiments are summarized in Table 1. Chemical shift index (CSI) analysis was performed according to the approach established by Wishart et al., adjusting the chemical shift reference of ^{13}C atoms to dioxane.[33]

Structure Calculation. Structure calculation of the Ni^{2+}−$H2B_{105-112}$ complex was performed using CYANA (version 2.1)[34] software on the basis of NOE and ROE signals, observed in the 2D-NOESY and ROESY spectra at pH 10.3, as described elsewhere.[20] A well-resolved restricted structure of the binding site, containing eight neighboring amino acids, from Glu_{12} to Ser_{19}, was determined. The 20 conformers with the lowest target function and NOE violations constitute the final family. The mean structure, obtained with MOLMOL software,[35] was then optimized, using the Amber force field implemented in Hyperchem 7.01, through an energy minimization in vacuo, using the Polak-Ribiere conjugate gradient method.[36] The structure calculations were performed using the e-NMR infrastructure,[37] and structure analysis and visualization were achieved by PyMol software.[38]

Hydrolytic Studies. Possible Ni^{2+}-assisted hydrolysis of $H2B_{94-125}$ was checked at physiological (pH 7.4) and experimental conditions (pH 10.3, where the formation of the 4N complex reaches its maximum with concominant total consumption of free Ni^{2+} ions), through HPLC and NMR, respectively. The latter was performed within the NMR tube containing a Ni:$H2B_{94-125}$ solution at a molar ratio of 1:1 with a ligand concentration of 2.5 mM. The solution was incubated at 37 °C, and several ^{1}H NMR spectra were recorded for up to 5 days.

For the hydrolysis study at physiological pH, solutions containing $H2B_{94-125}$ (0.3 mM) and/or $NiCl_2$ (0 or 0.3 mM) in 50 mM PBS (pH 7.4, K_2HPO_4/NaH_2PO_4, 0.15 M NaCl) were prepared and incubated at 37 °C for up to 5 days. Regularly, a 25 μL aliquot was removed and subjected to HPLC analysis on a Dionex P580 HPLC system, equipped with a Nucleosil 100 C_{18} 5 μM (250 mm × 4.6 mm) analytical column and UV detection at 220 and 214 nm.

In all cases, no new NMR peaks or new product formation was observed, suggesting a strong resistance in nickel-induced

(30) Irving, H. M. N. H.; Miles, M. G.; Pettit, L. D. *Anal. Chim. Acta* **1967**, *38*, (4), 475−488.
(31) Gans, P.; Sabatini, A.; Vacca, A. *Talanta* **1996**, *43*, (10), 1739−1753.
(32) Keller, R.; Wuthrich, K. *Computer Aided Resonance Assignment* (*CARA*). Available from: www.nmr.ch.
(33) Wishart, D. S.; Sykes, B. D.; Richards, F. M. *J. Mol. Biol.* **1991**, *222*, (2), 311−333. Wishart, D. S.; Sykes, B. D.; Richards, F. M. *Biochemistry* **1992**, *31*, (6), 1647−1651. Wishart, D. S.; Sykes, B. D. *J. Biomol. NMR* **1994**, *4*, (2), 171−180. Wishart, D. S.; Case, D. A. *Methods Enzymol.* **2001**, *338*, , 3−34.
(34) Guntert, P.; Mumenthaler, C.; Wuthrich, K. *J. Mol. Biol.* **1997**, *273*, (1), 283−298.
(35) Koradi, R.; Billeter, M.; Wuethrich, K., *J. Mol. Graph.* **1996**, *14*, (1), 51−55, plates, 29−32.
(36) Froimowitz, M. *BioTechniques* **1993**, *14*, (6), 1010−1013.
(37) e-NMR infrastructure, CERM Magnetic Resonance Center. http://www.cerm.unifi.it/home/research/onlinecalculations.html.
(38) Delano, W. L. *The PyMol molecular graphics system.* http://www.pymol.org.

Table 2. Protonation Constants and pK_α Values of Acidic Groups of $H2B_{94\text{-}125}$, T = 298 K (I = 0.2 M KCl)[a]

Protonation Constants (log β)							
HL	H_2L	H_3L	H_4L	H_5L	H_6L	H_7L	H_8L
11.65(9)	22.30(5)	32.59(8)	42.51(7)	51.65(7)	57.96(7)	62.32(7)	66.00(7)
pK_α Values							
p$K_{Glu}{}^1$	p$K_{Glu}{}^2$	pK_{His}	p$K_{Tyr/Lys}$	p$K_{Tyr/Lys}$	p$K_{Tyr/Lys}$	p$K_{Tyr/Lys}$	p$K_{Tyr/Lys}$
3.68	4.36	6.31	9.14	9.92	10.29	10.65	11.65

[a] Standard deviation of the last digit is given in parentheses.

hydrolysis of the $H2B_{94-125}$ fragment. This is in accordance with our previous findings,[28] requiring a Ser or Thr residue to be present near the Ni^{2+} coordination site to result in peptide hydrolysis. This is also in agreement with Karaczyn et al.'s observations,[22] concerning the whole H2B protein molecule.

Results

Characterization of the Free Ligand in Solution. The protonation constants (log β) and pK_α values of the acidic groups of $H2B_{94-125}$ were determined upon its potentiometric titration with KOH and are listed in Table 2. It must be mentioned that the calculated values are in good agreement with the ones calculated for peptides, containing Glu, Lys, and His residues in their sequence.[14,19,39]

The peptide $H2B_{94-125}$ may be considered as an H_8L ligand, owing to the presence of one His, two Glu, one Tyr, and four Lys residues. The pK_α values for the ionization of the phenolic ring of the Tyr residue and the ε-NH_2 of the four Lys residues are very close and cannot be assigned unambiguously to any of them. However, an evaluation can be made by the absorption spectra (Figure 1) that were recorded for the $H2B_{94-125}$ peptide, at different pH values.

As observed in Figure 1, the absorption in the ultraviolet region changes dramatically as the pH increases from 7.7 to 11.3. Particularly, the molar absorptivity increases in the region close to 250 nm, and a shift of the λ_{max} from 275 to 293 nm is observed. These changes are attributed to the ionization of the phenolic ring of the Tyr residue.[40] For the spectra in the alkaline region, two isosbestic points may be observed (271 and 277 nm), suggesting the presence of two different species. However, assuming the microscopic dissociation scheme, probably the different microspecies with protonated ε-NH_2 Lys cause the occurrence of a nonclear isosbestic point. On the other hand, the spectra recorded at the pH region 2.8−7.7 do not present any shift of the λ_{max} value, indicating that only the protonated form of the Tyr is present at this pH range.

The microconstant pK_α = 9.38, describing the ionization of the phenolic group, was calculated by the molar absorptivity at 300 nm. This value cannot be smaller than the macroconstant determined by potentiometry, since all microspecies, comprising the same stoichiometry but

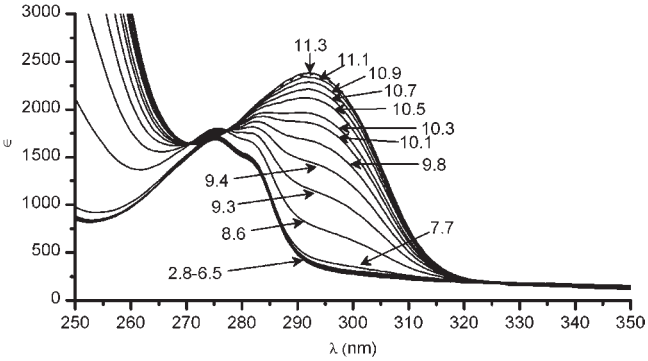

Figure 1. Absorption spectra of $H2B_{94-125}$ with changing pH.

different ionizable groups, contribute to the deprotonation step. Additionally, the macroconstant is the sum of all microconstants of all microspecies that are present at equilibrium.[40] The calculated macroconstant pK_α = 9.14 is the only one that is lower than the calculated microconstant. It thus seems logical to claim that at pH = 9.14 the concentration of peptide with deprotonated phenolic group is higher than the quantity of peptide comprising any of the deprotonated Lys ε-NH_2 groups and protonated phenolic ring.

The conformation of the free ligand in solution was studied by NMR spectroscopy at two extreme pH values (2.5 and 10.3). This was achieved by the assignment of resonances of $^1H_\alpha$, $^{13}C_\alpha$, and $^{13}C_\beta$ nuclei and use of the chemical shift index, as described by Wishart et al.[33] The analysis (Figure 2) indicates that at both pH values the peptide does not present secondary structure elements of an α-helix or β-strand, but rather adopts a random coil configuration.

Coordination Properties of Ni−$H2B_{94-125}$ Complexes. The potentiometric data were best fitted assuming the formation of nine species ($NiLH_5$, $NiLH_4$, $NiLH_3$, $NiLH_2$, NiLH, NiL, $NiLH_{-1}$, $NiLH_{-2}$, $NiLH_{-3}$), in the pH range 5 to 11.5. The formation constants (log β) and pK_α values were calculated with the Hyperquad software and are listed in Table 3. The log K* values correspond to the protonation-corrected stability constants, which are useful in comparing the ability of various ligands to bind a metal ion.[41] The spectroscopic data of each complex formed, which are given in Table 4, were estimated from the absorption and CD spectra (Figure 3) that were recorded at pH values where each complex reaches its maximum population, as evaluated by the species distribution diagram (Figure 4).

The species distribution diagram indicates that complexation of Ni^{2+} with $H2B_{94-125}$ begins at pH around 5 with the formation of the $NiLH_5$ species. This complex cannot be detected spectroscopically, due to its low concentration (at pH 7.4 it accounts for complexation of only 10% of total nickel concentration). However, it can be characterized on the basis of its stoichiometry and stability constant. The log K* values fit perfectly with those of the smaller fragment ELAKHA (Table 3), contained within the sequence $H2B_{94-125}$ and are comparable with the ones given in the literature for the 1N

(39) Kowalik-Jankowska, T.; Rajewska, A.; Wisniewska, K.; Grzonka, Z.; Jezierska, J. *J. Inorg. Biochem.* **2005**, *99*, (12), 2282−2291.
(40) Motekaitis, R. J.; Martell, A. E.; Martell, A. E.; Motekaitis, R. J. *The Determination and Use of Stability Constants*; VCH Publishers: New York, 1988.
(41) Bal, W.; Dyba, M.; Kasprzykowski, F.; Kozlowski, H.; Latajka, R.; Lankiewicz, L.; Mackiewicz, Z.; Pettit, L. D. *Inorg. Chim. Acta* **1998**, *283*, (1), 1−11.

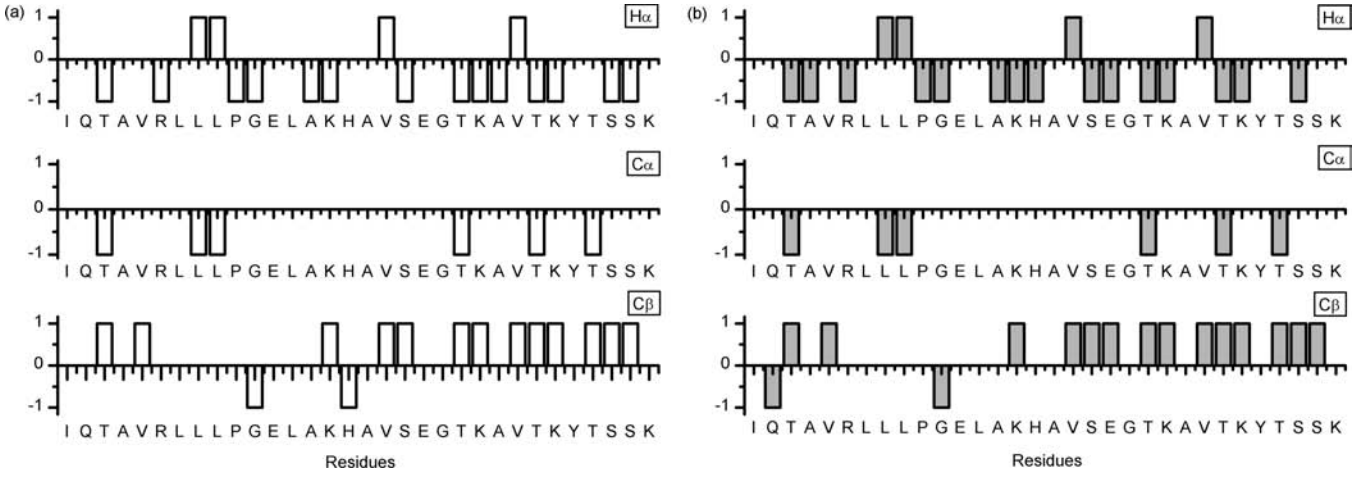

Figure 2. CSI plots for $H2B_{94-125}$ at pH (a) 2.5 (white) and (b) 10.3 (gray). The consensus plots are omitted due to the fact that all values are equal to zero.

Table 3. Stability Constants of Nickel Complexes with $H2B_{94-125}$, T = 298 K, I = 0.2 M (KCl)

Stability Constants (log β)[a]								
$NiLH_5$	$NiLH_4$	$NiLH_3$	$NiLH_2$	NiLH	NiL	$NiLH_{-1}$	$NiLH_{-2}$	$NiLH_{-3}$
54.1(1)	46.21(8)	37.20(2)	29.13(3)	19.82(2)	10.05(2)	−0.28(2)	−10.92(2)	−22.14(2)

Ionization Constants (pK_α)							
$NiLH_5$	$NiLH_4$	$NiLH_3$	$NiLH_2$	NiLH	NiL	$NiLH_{-1}$	$NiLH_{-2}$
$NiLH_4$	$NiLH_3$	$NiLH_2$	NiLH	NiL	$NiLH_{-1}$	$NiLH_{-2}$	$NiLH_{-3}$
7.89	9.01	8.07	9.31	9.77	10.33	10.64	11.22

log K*[b]				
	1N {N_{Im}}	2N {N_{Im}, N^-_{amide}}	3N {N_{Im}, $2N^-_{amide}$}	4N {N_{Im}, $3N^-_{amide}$}
$H2B_{94-125}$	−3.86	−11.75	−20.76	−28.83
ELAKHA	−3.55	−11.75		−28.87

[a] $\beta_j = [MH_jL]/[M][H^+]^j[L]$. [b] $\log K^* = \log \beta(MLH_j) - \log \beta(H_6L)$.

complexes of Ni^{2+} with Ac-TRSRSHTSEGTRSR-Am (log K^* = −3.62)[42] and Ac-AKRHRK-Am (log K^* = −4.02)[14] peptides, suggesting the same coordination mode. In all cases, the His residue provides through the N(3) imidazole nitrogen an efficient anchoring site, leading to the formation of distorted octahedral complexes {N_{Im}}.

By raising the pH, $NiLH_5$ releases a proton, forming $NiLH_4$. The pK_α value (7.89) for this deprotonation process is typical for the first amide deprotonation. Moreover, the value log K^* = −11.75 is characteristic for the formation of a 2N {N_{Im}, N^-} species.[13,14,16,19] This is further supported by the presence of the maximum at positive $\Delta\varepsilon$ values, in the CD spectra, recorded at pH 8.3 (Figure 3), which is characteristic of the formation of a six-membered chelate ring by the histidine residue.[43] The charge transfer band at 255 nm may be attributed to the transition $N_{Im} \rightarrow Ni^{2+}$, while an additional band at 269 nm is likely to involve the $N^-_{amide} \rightarrow Ni^{2+}$ transition.[9]

The next formed species $NiLH_3$ cannot be detected spectroscopically due to its low concentration and overlap with species $NiLH_4$ and $NiLH_2$. Nevertheless, potentiometry suggests its existence in the pH range 7.8−9.6. The thermodynamic parameters given in Table 3 are typical for the ionization of an extra amide nitrogen and the complexation of the ion with a {N_{Im}, $2N^-_{amide}$} donor set.[42] It is also noteworthy that the ionization of the third amide nitrogen that leads to the formation of the $NiLH_2$ species occurs with a pK_α value (8.07) that is lower than the one calculated for the second amide deprotonation (9.01). This is indicative of the highly cooperative character of the above-mentioned ionizations and explains the low concentration of the $NiLH_3$ species.

The thermodynamic parameters and spectroscopic data given in Tables 3 and 4, respectively, for the complexes with stoichiometry $NiLH_2$ suggest that this species is a 4N square-planar diamagnetic complex, where the metal ion is coordinated with the N(3) imidazole and three amide nitrogens from the backbone of the peptide {N_{Im}, $3N^-_{amide}$}.[16−19] The pK_α values that were calculated for the subsequent deprotonation steps are very close to the ones calculated for the ionization of the phenolic ring and ε-NH_2 of Tyr and Lys residues, respectively. The latter and also the fact that the shape of the absorption and CD spectra recorded at pH > 9 does not change indicate that the geometry and coordination mode of the $NiLH_2$, NiLH, NiL, $NiLH_{-1}$, and $NiLH_{-2}$ complexes are identical. Likewise, the fact that the value pK_α = 9.31 for the deprotonation process $NiLH_2$/NiLH agrees

(42) Zoroddu, M. A.; Kowalik-Jankowska, T.; Kozlowski, H.; Salnikow, K.; Costa, M. *J. Inorg. Biochem.* **2001**, *84*, (1−2), 47−54.
(43) Chang, J. W.; Martin, R. B. *J. Phys. Chem.* **1969**, *73*, (12), 4277−4283.

fairly with the calculated microconstant for the Tyr residue (pK_α = 9.38) suggests that the first proton in the 4N complex is liberated mostly from the noncoordinating phenolic OH.

NMR Study of the 4N Complex. As seen by the species distribution diagram (Figure 4), the pH choice for the NMR study of the 4N complex is not an easy task. The presence of four Lys and one Tyr residue in the peptide's sequence with approximately the same pK_α values results in the formation of several complexes in the pH-metric region 8−11.5. This does not allow the conduction of the NMR experiments at a discrete pH value, where a unique 4N complex predominates. The selection gets more limited due to the fact that above pH 11.5 precipitation was observed. However, on the basis of the fact that the coordination mode and geometry of the $NiLH_2$, NiLH, NiL, $NiLH_{-1}$, and $NiLH_{-2}$ species do not change, we decided to record the NMR spectra at pH 10.3. Furthermore, at this pH there is no free paramagnetic nickel, which may cause broadening of the bands and decrease in the quality of the recorded spectra. It must be considered that at this pH in most of the present species the Tyr residue is deprotonated.

The assignment of the ^1H and ^{13}C resonances was achieved by the combined analysis of the TOCSY, ^{13}C-HSQC, NOESY, and ROESY spectra that were recorded for the free and Ni^{2+}-bound peptide, at pH 10.3. At this pH, the rapid exchange of the labile amide protons with protons from the solvent molecules does not allow the observation of their resonance signals. In order to facilitate the assignment process, we recorded a series of ^{15}N-HSQC, TOCSY, ^{13}C-HSQC, NOESY, and 3D NHHa spectra at pH 2.5, where the exchange rate is low and the amide protons' signals may be observed in the NMR time scale.

The progressive saturation of the binding site by the metal ion was monitored by the titration of the peptide with nickel ions at pH 10.3 (Figure 5). In the absence of the metal the only signals observed above 6 ppm are those attributed to the imidazole and phenolic protons of the

Table 4. Spectroscopic Data for Ni^{2+} Complexes with $H2B_{94-125}$, at 298 K

	UV−vis		CD	
species	λ_{max} (nm)	ε (M^{-1} cm^{-1})	λ_{max} (nm)	$\Delta\varepsilon$ (M^{-1} cm^{-1})
$NiLH_5$ (1N)[a]				
$NiLH_4$ (2N)			255[b]	+1.40
			269[d]	+0.30
			416[c]	−0.51
			513[c]	+0.17
$NiLH_3$ (3N)[a]				
$NiLH_2$ (4N)	428	134	255[b]	+3.70
			274[d]	+1.34
			417[c]	−1.75
			510[c]	+0.84
NiLH (4N)	433	177	256[b]	+6.65
			274[d]	+2.53
			418	−3.05
			514	+1.48
NiL (4N)			252[b]	+7.54
			273[d]	+2.84
			418[d]	−3.34
			514[d]	+1.57
$NiLH_{-1}$ (4N)	433	185		
$NiLH_{-2}$ (4N)	433	191	254[b]	+8.46
			276[d]	+3.01
			418[d]	−3.59
			514[d]	+1.76
$NiLH_{-3}$ (4N)	433	200	253[b]	+8.26
			274[d]	+2.98
			418[d]	−3.67
			514[d]	+1.79

[a] Not detected due to its low concentration or overlap with other species. [b] Charge transfer band $N_{Imidazole} \rightarrow Ni^{2+}$. [c] d−d transition. [d] Charge transfer band $N_{amide} \rightarrow Ni^{2+}$.

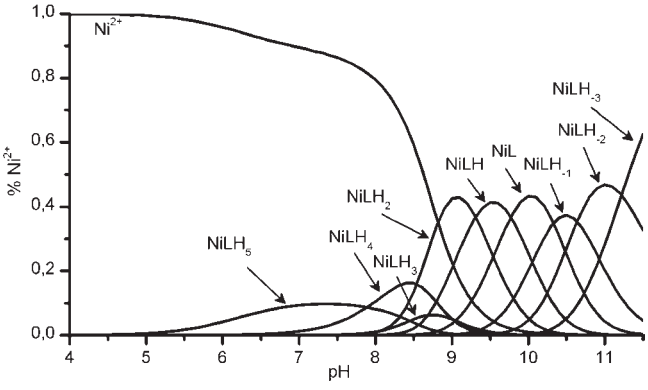

Figure 4. Species distribution diagram of the Ni^{2+}−$H2B_{94-125}$ system at a molar ratio of 1:1.1, using the stability constants obtained from potentiometry.

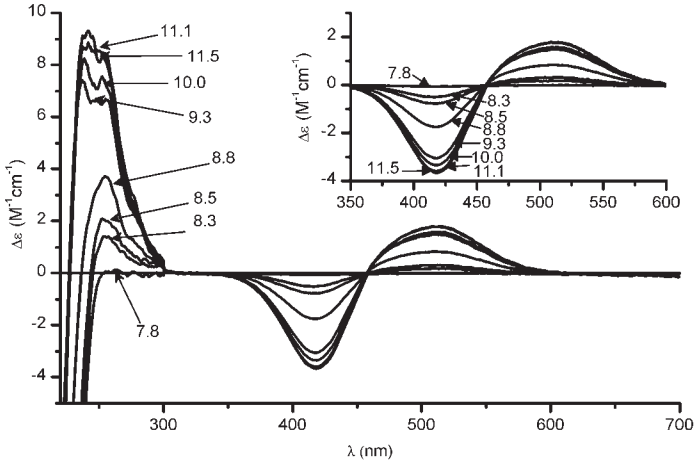

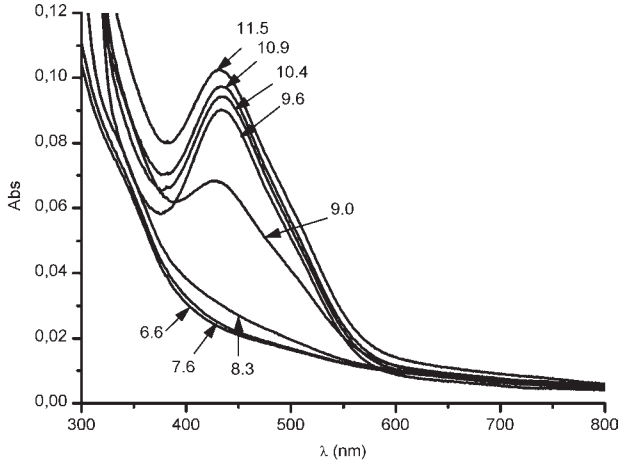

Figure 3. CD and UV−vis spectra of the $H2B_{94-125}$−Ni^{2+} system as a function of pH.

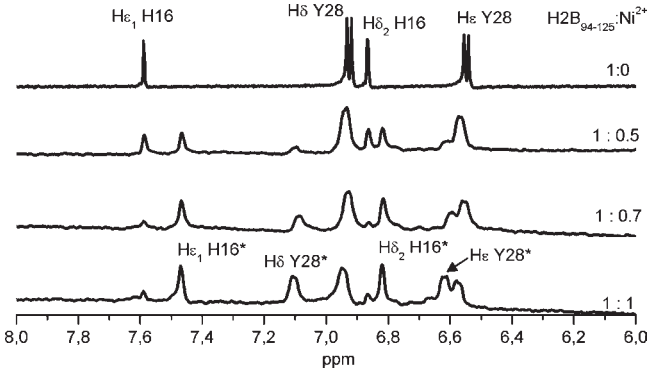

Figure 5. Aromatic region of ^{1}H NMR spectra collected at 600 MHz, 298 K at pH 10.3 of $H2B_{94-125}$ peptide with increasing amounts of Ni^{2+} from 0 equiv (free peptide) to 1 equiv. New peaks resulting from Ni^{2+} addition are labeled with an asterisk. Broadening of the peaks in the Ni^{2+}-bound spectra is attributed to the paramagnetic octahedral complexes initially formed.[28]

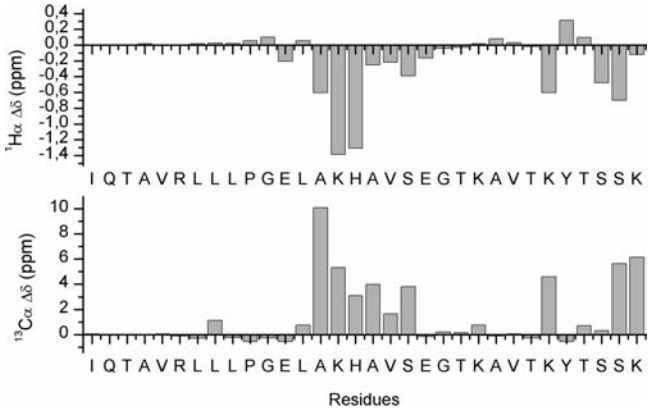

Figure 6. Graphical representation of the $^{1}H_{\alpha}$ and $^{13}C_{\alpha}$ chemical shift difference between Ni^{2+}-bound and free $H2B_{94-125}$, in a molar ratio of peptide to metal of 1:1, at pH 10.3, 298 K.

His and Tyr residue, respectively. Nickel titration results in the progressive shifting of the above-mentioned signals. Especially, the intensity of the $H_{\varepsilon 1}$ and $H_{\delta 2}$ proton signals, observed at 7.59 and 6.86 ppm, respectively, gets reduced, while at the same time, two new signals at 7.47 and 6.82, corresponding to those protons in the new environment of the complex, appear with a progressive increase in their intensity. It is noteworthy that the signals of the aromatic phenolic protons are also shifted, indicating that the local environment of Tyr_{28} is also somehow affected upon nickel binding.

The assignment of the cross-peaks in the Ni^{2+}-bound spectra was achieved by comparing with those of the free ligand. The new cross-peaks observed upon nickel addition were attributed to the $Ni^{2+}-H2B_{94-125}$ complex. The chemical shift differences of the α-protons and α-carbons between the Ni^{2+}-bound and unbound peptide state are shown in Figure 6. The complete resonance assignments of ^{1}H, ^{13}C, and ^{15}N nuclei are given in Tables S1 and S2, as Supporting Information (SI). Overlaid aliphatic region and H_{α}-C_{α} region of free and Ni^{2+}-bound peptide of TOCSY and ^{13}C-HSQC spectra, respectively, are given as Figures S1 and S2 in the SI.

The addition of Ni^{2+} ions in the peptide's solution causes selective shifting of the ^{1}H and ^{13}C resonance signals of several residues (Figures 6 and S2). The largest

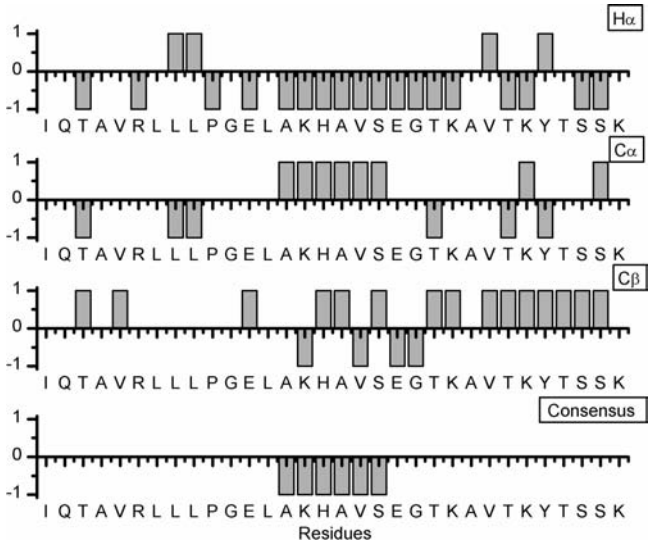

Figure 7. CSI plots for Ni^{2+}-bound peptide at pH 10.3.

changes are observed as upfield shifts of the α-protons of His_{16}, Lys_{15}, and Ala_{14}, indicating that this portion of the peptide is mostly involved in the coordination process. Likewise, lower shifting of ^{1}H and ^{13}C resonance signals is observed for the neighboring residues Glu_{12}, Leu_{13}, Ala_{17}, Val_{18}, Ser_{19}, and Glu_{20}, suggesting that the magnetic environment of those nuclei is also modified upon nickel binding. More important may be the fact that Ni^{2+} binding causes severe changes in the ^{1}H and ^{13}C resonance signals of the residues, composing the C-terminal tail fragment Lys_{27}-Tyr_{28}-Thr_{29}-Ser_{30}-Ser_{31}-Lys_{32}, thus evidencing a different chemical environment for this portion, compared to the one of the unbound peptide.

CSI analysis for Ni^{2+}-bound peptide (Figure 7) indicates a conformational change for the $-A_{14}KHAVS_{19}-$ fragment. We are aware of the fact that the high pH may influence the method's sensitivity. Likewise, nickel coordination may cause a general upfield or downfield tendency in the chemical shifts. However, our data suggest a conformational change for this fragment that is unlikely to be a transition from a random coil configuration to an α-helix secondary structure, as assessed by the consensus diagram, but more likely to appear due to the adoption of a unique backbone geometry upon complex formation.

The H_{α} proton of His_{16} presents a severe upfield shift ($\Delta\delta > 1$ ppm). Upfield shifts are also observed for the β and aromatic protons of the imidazole ring (Figure S2). These observations are in accordance with the important anchoring role of the His residue in coordination studies of metal ions with peptides comprising one His residue in their sequence.[9,12,16,17,20,27] A larger chemical shift difference is observed only for the H_{α} proton of Lys_{15} ($\Delta\delta = -1.39$), suggesting that this residue belongs to the binding site, as well. The fact that the resonance signals of β- and δ-protons of this particular residue appear separated upon nickel binding (Table S2) is also noteworthy. This can be explained through the enforcement of a more "strict" conformation, due to complex formation, which limits their free movement. The H_{α} proton of Ala_{14} also presents a substantial shifting. The value $\Delta\delta = -0.60$ may be comparable to the ones observed for the H_{α} protons of Lys_{27} ($\Delta\delta = -0.61$) and Ser_{32} ($\Delta\delta = -0.70$), but

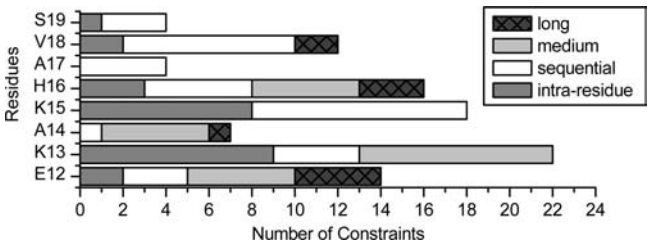

Figure 8. Schematic representation of the number of meaningful NOE constraints per residue for the $H2B_{94-125}-Ni^{2+}$ complex used in the structural calculations.

the downfield shift of the C_α nuclei for this residue is the largest observed among all (Figure 6).

These changes in the chemical shifts may be explained by the binding of the metal with the portion Ala_{14}-Lys_{15}-His_{16} and confirm the potentiometric and spectroscopic results obtained earlier. Potentiometry and the unique characteristics of the UV−vis and CD spectra suggest a $\{N_{Im}, 3N^-_{amide}\}$ donor set. NMR spectroscopy indicates that the coordinated amide nitrogens belong to the above-mentioned residues. The formation of a six- and three five-membered chelate rings is the driving force for 4N complex formation.

As said before, the formation of the 4N complex at alkaline pH does not allow the observation of the amide protons' resonance signals, due to fast exchange. This lack of evidence almost forbids the generation of a well-defined structure. However, on the basis of the NOE signals generated by the interaction of side chain protons, we managed to determine a well-resolved restricted structure for the binding site, containing the octapeptidic fragment -Glu_{12}-Leu_{13}-Ala_{14}-Lys_{15}-His_{16}-Ala_{17}-Val_{18}-Ser_{19}-. For this reason we used 61 meaningful upper distance limits (available in Table S3 of the SI), including 25 intraresidual, 15 sequential, 16 medium, and 5 long-range (Figure 8), together with the geometric constraints for the Ni^{2+} ion that were extracted from the crystal structure of the analogous complex, Ni^{II}(Gly-Gly-α-hydroxyl-D,L-histamine)]·$3H_2O$.[44] For this fragment, a total of 86.5% of assigned atoms was determined. The obtained structure family has an average total target function of 0.19 ± 0.0025 Å^2 and rmsd of 0.15 ± 0.03 and 0.31 ± 0.07 Å for the backbone and heavy atoms, respectively. The proposed structures show a $\{N_{Im}, N^-_{H16}, N^-_{K15}, N^-_{A14}\}$ donor set (Figure 9). The molecular dynamics force field used for geometry optimization of the mean structure took into account, besides the NMR-derived distance constraints, bond stretching, angle and dihedral bending terms, and electrostatic and van der Waals interactions, thus improving the position of the metal in the coordination plane (Figure 9b).

Discussion

Potentiometry suggests the formation of several complexes between nickel ions and the $H2B_{94-125}$ ligand. The thermodynamic data, listed in Table 3, indicate that their stability is very close to that reported in the literature for the analogous complexes of nickel with the hexapeptide (containing the binding site) ELAKHA,[17] suggesting the same coordination modes. The log K^* values imply that the 1N $\{N_{Im}\}$ complex of −ELAKHA− is more stable than the analogous $Ni^{2+}-H2B_{94-125}$ complex. For the ELAKHA complex a possible participation of the carboxyl group of the Glu residue was proposed,[17] and this cannot be excluded for the $H2B_{94-125}$ peptide. It is also noteworthy that in the case of the $H2B_{94-125}$ peptide model potentiometry indicates the existence (although in very small amounts) of the 3N complex. Although this can be an artifact of the simulation software, it may be an evidence for a slower kinetics of the spin pairing process, during the transition from a 2N to a 4N complex, owing to an extra rearrangement of the side chain groups of $H2B_{94-125}$. This would allow the formation of detectable amounts of the 3N complex and reduce the synergistic character of the second and third amide ionization compared with ELAKHA.

The examination of the 4N complex's structure reveals that the backbone of Ala_{17}, Val_{18}, and Ser_{19} is placed right over the coordination plane (Figure 9). This fact explains the upfield shifts of their α-protons upon nickel binding, since they get more shielded by the electronic-rich environment of the complex. Moreover, the positions of the hydrophobic side chain groups of Ala_{17} and Val_{18} protect the complex from the axial nucleophilic attack of water molecules or H^+ from the bulk of the solution to the Ni^{2+}-amide nitrogens. Additionally the space below the coordination plane is filled with the bulky side chain group of Leu_{13}. Interestingly, the H_α proton of this residue is placed far away from the metal, being oriented to the bulk of the solution. This may be responsible for the downfield shift observed for this nucleus, upon nickel coordination.

As assessed by Figure 6, the chemical shift difference for the α-protons of the residues composing the binding site follows the order H_α (Lys_{15}) > H_α (His_{16}) > H_α (Ala_{14}). The examination of the obtained structures reveals that the distance between those atoms and the metal ion is H_α (Lys_{15})$-Ni^{2+}$ (3.61−3.62 Å), H_α (His_{16})$-Ni^{2+}$ (4.30−4.31 Å), and H_α (Ala_{14})$-Ni^{2+}$ (2.98−3.00 Å) (Figure 10). According to the above, it is easy to explain the larger shifting of the Lys α-proton resonance signal, since it is more shielded by the metal ion. The fact that the $\Delta\delta$ value for the α-proton of the Ala_{14} residue is quite small, although situated very close to the metal, can be attributed to a structural characteristic that may induce a deshielding effect. A closer look at the structure reveals a possible interaction between the carbonyl oxygen of Val_{18} and the α-proton of Ala_{14}. Indeed, the distance between those two nuclei does not exceed 2.35 Å in 12 out of the 20 structures of the final family. Those two atoms are rather distant from each other, being unlikely to form a hydrogen bond;[45] nevertheless their increased incidence of contact may assist in a deshielding effect experienced by the α-proton. This interaction could be responsible for the shifting of the α-proton resonance signal in lower field than expected.

Unfortunately, the lack of meaningful NOE signals did not allow the generation of a well-defined structure for the whole peptide$-Ni^{2+}$ complex. However, it is quite interesting that besides the residues composing or being close to the binding site, profound shifting of the resonance signals is observed for the proton and carbon nuclei of residues Lys_{27}, Tyr_{28}, Thr_{29},

(44) Bal, W.; Djuran, M. I.; Margerum, D. W.; Gray, E. T., Jr.; Mazid, M. A.; Tom, R. T.; Nieboer, E.; Sadler, P. J. *J. Chem. Soc., Chem. Commun.* **1994**, (*16*), 1889−1890.

(45) Guntert, P. *Q. Rev. Biophys.* **1998**, *31*, (2), 145−237.

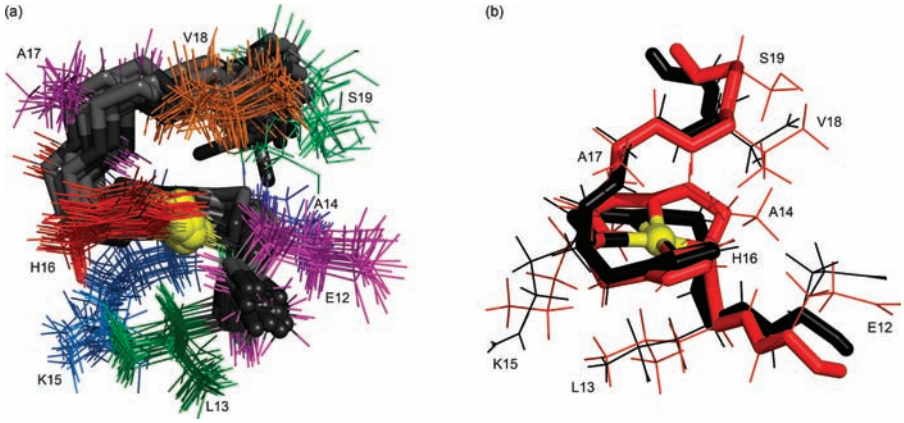

Figure 9. (a) Stereoview of superposition of the 20 lowest energy structures of Ni^{2+}−$H2B_{105-112}$ obtained from NMR data. (b) Overlaid mean (black, E = 9460.38 kcal mol^{-1}/gradient = 957.7 kcal mol^{-1} Å^{-1}) and geometric optimized (red, E = 168.6 kcal mol^{-1}/gradient = 0.09 kcal mol^{-1} Å^{-1}).

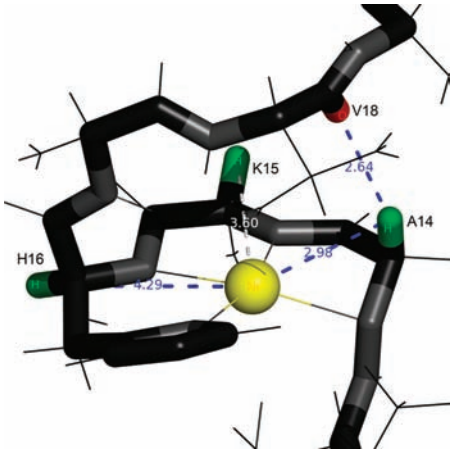

Figure 10. Enlargement of the binding site in the mean structure. The distances given are in angstroms (color code: Ni^{2+} yellow, H_α of Ala_{14}, Lys_{15}, His_{16} green, carbonyl oxygen of Val_{18} red).

Ser_{30}, Ser_{31}, and Lys_{32} that compose the C-terminal tail of the peptide (Figure 6).

The potentiometric and spectroscopic data, presented in Tables 3 and 4, are typical for the coordination of the nickel ion with a $\{N_{Im}, 3N^-_{amide}\}$ donor set. Moreover, the absence of the characteristic charge transfer band at 420 nm in other experiments with Cu^{2+} that will be reported elsewhere, in the recorded CD spectra, suggests that the phenolic oxygen of Tyr_{28} does not coordinate to the metal. However, this residue presents a severe downfield shift for all its protons. The most profound chemical shift difference is observed for the β-proton resonance signals ($\Delta\delta$ = 0.89, $\Delta\delta$ = 0.45 ppm, cf. Table S2), which is accompanied by an increase in their separation. The latter suggests a decrease in their free movement, which allows their better separation in the NMR time scale. The same phenomenon is observed for the γ-protons of Lys_{27}, which upon complexation appear well separated. It is thus evident that Ni^{2+} coordination leads to a more organized structure for Lys_{27} and Tyr_{28}.

The most logical explanation of the above-mentioned observations is that nickel binding induces the adoption of a conformation where distant parts of the peptide molecule come close in space. The interactions being responsible for this may be of electrostatic nature and lead to a more thermodynamically stable structure. The phenolic oxygen of Tyr_{28} has a negative charge, which is able to interact with

Table 5. NOE Cross-Peaks between α and Side Chain Protons of Binding Site and Neighboring Residues and Protons of the C-Terminal Tail K_{27}-Y_{28}-T_{29}-S_{30}-S_{31}-K_{32} of Ni^{2+}-Bound $H2B_{94-125}$ at pH 10.3

proton 1	proton 2	proton 1	proton 2
$H_{\varepsilon 1}$ His_{16}	Q_δ Lys_{27}	$H_{\delta 2}$ His_{16}	$H_{\beta 3}$ Tyr_{28}
H_α Lys_{15}	$H_{\delta 1}$ Tyr_{28}	$H_{\gamma 3}$ Lys_{15}	Q_ε Lys_{27}
H_α Lys_{15}	$H_{\delta 2}$ Tyr_{28}	Q_γ Val_{18}	H_α Ser_{30}
$H_{\delta 2}$ His_{16}	Q_γ Lys_{32}	H_α His_{16}	Q_β Ser_{30}
$H_{\delta 2}$ His_{16}	$H_{\beta 3}$ Tyr_{28}	$H_{\gamma 3}$ Lys_{15}	H_α Lys_{32}
$H_{\delta 2}$ His_{16}	H_β Thr_{29}	$H_{\gamma 2}$ Glu_{12}	Q_β Lys_{32}
H_α Lys_{15}	Q_ε Tyr_{28}	$H_{\gamma 2}$ Lys_{15}	Q_β Lys_{32}
$H_{\beta 3}$ His_{16}	$H_{\beta 3}$ Tyr_{28}	H_α Ser_{19}	Q_δ Lys_{32}

the electrostatic potential generated by the complex. This type of interaction, which may be considered as a salt bridge, has been reported in coordination studies of small peptides with Cu^{2+} and Pd^{2+},[46] as well as for the interaction of nickel with the peptide model of human protamine,[27] where the Tyr residue is separated by the anchoring His, through five residues. In our case the Tyr residue is much more distant from the His (separated by 11 residues in the peptide's sequence); however, the presence of the cross-peaks given in Table 5 in the ROESY (Figure 11) and NOESY spectra is indicative of the proximity of the C-terminal tail Lys_{27}-Tyr_{28}-Thr_{29}-Ser_{30}-Ser_{31}-Lys_{32} to the coordination plane.

Moreover, the severe upfield shift of Lys_{27} α-proton ($\Delta\delta$ = −0.61) suggests its proximity to the binding site. This is accompanied with a downfield shift of all side chain aliphatic protons, observed with a smaller $\Delta\delta$ value according to the order $\beta > \gamma > \delta > \varepsilon$ (cf. Table S2). It thus seems possible that the Lys_{27} side chain approaches the coordination plane pointing toward the metal. Additionally, the residues Ser_{30}, Ser_{31}, and Lys_{32} seem to approach the coordination plane close enough to present a substantial shifting of their α-protons. The fact that the ^1H and ^{13}C resonance signals of Thr_{29} are less affected upon Ni^{2+} binding may suggest that the fragment Ser_{30}-Ser_{31}-Lys_{32} turns around this residue while approaching the coordination plane.

Unfortunately, the lack of several meaningful NOE signals does not allow the generation of a precise structure that would include the C-terminal tail. Nevertheless, the data

(46) Bal, W.; Dyba, M.; Kozlowski, H. *Acta Biochim. Pol.* **1997**, *44*, (3), 467−476. Kozlowski, H.; Jezowska, M. *Chem. Phys. Lett.* **1977**, *47*, (3), 452−456. Van der Helm, D.; Franks, W. A. *J. Am. Chem. Soc.* **1968**, *90*, (20), 5627−5629. Kozlowski, H. *Inorg. Chim. Acta* **1978**, *31*, (1), 135−140. Amirthalingam, V.; Muralidharan, K. V. *Acta Crystallogr., Sect. B* **1976**, *B32*, (12), 3153−3156. Mosset, A.; Bonnet, J. J. *Acta Crystallogr., Sect. B* **1977**, B33, (9), 2807−2812.

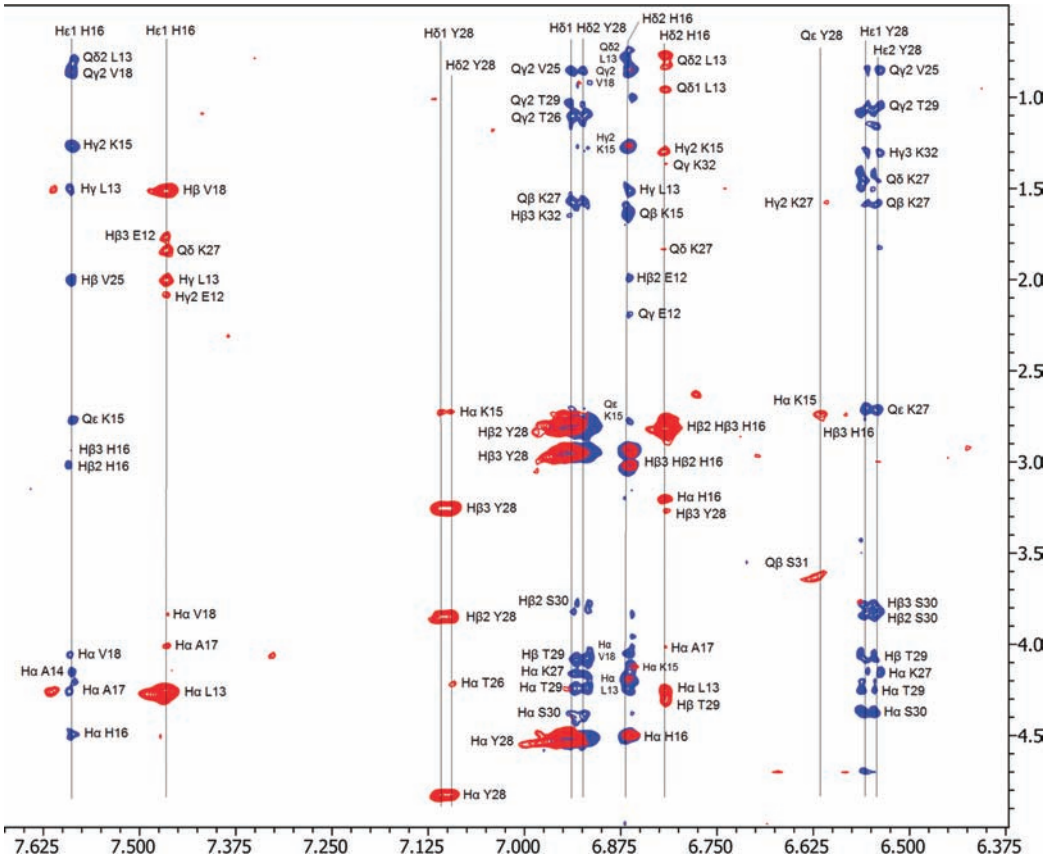

Figure 11. Overlaid aromatic region of ROESY spectra of free (blue) and Ni^{2+}-bound peptide (red).

presented above indicate a conformational change for this portion, due to its placement close to the binding site. We do not know if and to what extent the interaction of the negative charge of the phenolic oxygen with the electrostatic potential generated by the complex influences the adoption of such a structure. Indeed, dissociation of the tyrosine phenol group may not occur under physiological conditions due to the high pK_α value for this ionization process. However, phosphorylation of Tyr residues, which has been shown to occur often, under physiological conditions induces a negative charge that may have a similar effect.[47] Alternatively, stacking of the phenol group with the imidazole may stimulate analogous structural alterations for the C-terminal fragment. Aromatic ring stacking has been recognized as one of the most important interactions in stabilizing the tertiary structure in proteins and has been observed, for example, for the active sites of galactose oxidase[48] and cytochrome *c* oxidase.[49] In any case, if such a structural modification is possible under physiological conditions, it may be directly related with the process of nickel-induced carcinogenesis, since it involves Lys_{27}, which is the substrate of the ubiquitination process.

In the past years, this post-translational modification of histone H2B has been correlated with the activation of DNA transcription.[23] In general, ubiquitination refers to the binding of a ubiquitin molecule to the side chain of a Lys residue, through the formation of an isopeptidic bond between the carboxylate group of the C-terminal Gly residue of ubiquitin and side chain ε-NH_2 group of Lys. Although the way this modification functions is still unknown, it has been proposed that it leads to a wide open conformation of chromatin, which facilitates the approach and action of DNA transcription factors.[3] Additionally, there is evidence that $H2B/Lys_{120}$ ubiquitination is a necessary first step for the methylation of Lys_4 of histone H3. This methylation has been shown to have a role in gene silencing within heterochromatin. Therefore, the nonphysiological $H3/Lys_4$ methylation may lead to expression of telomeric genes.[24]

Our NMR data suggest that Ni^{2+} binding at His_{109} leads to a structural alteration of the C-terminal tail, which seems to adopt a more condensed conformation. This may have an impact on the recognition and/or ubiquitin binding process at Lys_{120} by the appropriate H2B K120 ubiquitilase. The arrangement of the Lys side chain group toward the metal supported by our NMR results would definitely confine the ε-NH_2 group to a restricted space, diminishing the approach of a large ubiquitin molecule. This may imply transcription errors, resulting in carcinogenesis.

Conclusions

The potentiometric and spectroscopic data of the $H2B_{94-125}/Ni^{2+}$ system presented in this study point out the fragment Ala_{14}-Lys_{15}-His_{16} as the main portion involved

(47) Kolata, G. *Science* (*Washington, D. C.*) **1983**, *219*, 377–378. Ingebritsen, T. G.; Cohen, P. *Science* (*Washington, D. C.*) **1983**, *221*, 331–338. Brand, S. J.; Anderson, B. N.; Rehfeld, J. F. *Nature* (*London*) **1984**, *309*, 456–458.

(48) Ito, N.; Phillips, S. E. V.; Stevens, C.; Ogel, Z. B.; McPherson, M. J.; Keen, J. N.; Yadav, K. D. S.; Knowles, P. F. *Nature* **1991**, *350*, 87. Itoh, N.; Phillips, E. V.; Yadav, K. D. S.; Knowles, P. F. *J. Mol. Biol.* **1994**, *238*, 794.

(49) Tsukihara, T.; Aoyama, H.; Yamashita, E.; Tomizaki, T.; Yamaguchi, H.; Shinzawa-Itoh, K.; Nakashima, R.; Yaono, R.; Yoshikawa, S. *Science* **1995**, *269*, 1069. Yoshikawa, S.; Shinzawa-Itoh, K.; Nakashima, R.; Yaono, R.; Yamashita, E.; Inoue, N.; Yao, M.; Fei, M. J.; Libeu, C. P.; Mizushima, T.; Yamaguchi, H.; Tomizaki, T.; Tsukihara, T.; Aoyama, H. *Science* **1998**, *280*, 1723. Iwata, S.; Ostermeier, C.; Ludwig, B.; Michel, H. *Nature* **1995**, *376*, 660.

in the coordination process. Likewise, the placement of the hydrophobic side chains of Ala_{17} and Val_{18} above as well as the position of the bulky aliphatic group of Leu_{13} below the coordination plane are the main interactions that stabilize the 4N $\{N_{Im}, 3N^{-}\}$ complex.

Ni^{2+} binding does not result in the hydrolysis of the peptide, as expected,[28] but in a severe conformational change, not only for the binding site but also for the C-terminal tail of the peptide. Therefore, it may be possible that metal binding at His_{109} and the resulting conformational effect may have a distinct impact on the nucleosome dynamics and particularly on the ubiquitination of Lys_{120}.

We do not know if Ni^{2+} binding at His_{109}, followed by structural alteration of the C-terminal tail, may take place under physiological conditions, since our NMR study was restricted to a strong alkaline pH. Under our experimental conditions the formation of the 4N complex starts at pH 8 and reaches maximum formation for the $NiLH_2$ species at pH 9. However, it is likely that the different conditions within cells as well as the hydrophobic environment in the whole protein increase metal binding efficiency, either by multiple nonbonding interactions available there or due to a higher selectivity of nickel in inducing a certain conformation of the peptide.[29]

We believe that this study may assist in the interpretation of ubiquitination efficiency loss in cells treated with Ni^{2+} and give a better insight in the mechanisms of metal-induced carcinogenesis.

Acknowledgment. This research project is co-funded by the European Union−European Social Fund (75%) and 25% by National Sources (Ministry of Development, General Secretarial of Research and Technology of Greece) in the framework of measure 8.3 of the operational programme "Competiveness" of the 3rd Community Support Framework (PENED 2003). The access to the NMR and to the e-NMR infrastructures, CERM (Florence), was supported by the EU projects EUNMR (contract no. RII3 026145) and contract 213010.

Supporting Information Available: Chemical shifts for ^{1}H, ^{13}C, and ^{15}N nuclei at pH 2.5 (Table S1). Aliphatic region of the $[^{1}H-^{1}H]$-TOCSY of the free and Ni^{2+}-bound $H2B_{94-125}$ at pH 10.3 (Figure S1). Chemical shifts and chemical shift difference for ^{1}H and ^{13}C nuclei of $H2B_{94-125}$, in the free and Ni^{2+}-bound state, at pH 10.3 (Table S2). Hα-Cα region of the $[^{1}H-^{13}C]$-HSQC of the free (red) and Ni^{2+}-bound $H2B_{94-125}$ (green). New resonances due to Ni^{2+} binding have been labeled (Figure S2). Constraints used for structure determination (Table S3). This material is available free of charge via the Internet at http://pubs.acs.org.